


Article

Optimisation of Control Strategies for Power Shift Gearboxes

Wenlong Pan ^{1,2}, Lei Wang ^{2,*}, Xiangdong Ni ^{1,2}, Wenqing Cai ³, Yongqiang Zhao ¹, Huajun Chen ¹ ,
Yuangang Lin ¹ and Yuhan Zhou ¹

¹ College of Mechanical and Electrical Engineering, Shihezi University, Shihezi 832003, China; 15037404808@163.com (W.P.); nini0526@126.com (X.N.)

² Key Laboratory of Modern Agricultural Machinery, Xinjiang Production and Construction Corps, Shihezi 832000, China

³ College of Information Science and Technology, Shihezi University, Shihezi 832003, China; cwq0526@sohu.com

* Correspondence: wl_mac@shzu.edu.cn

Abstract: This study is based on the influence of power shift control on the smoothness of cotton picker shifts and proposes an optimization method for the smoothness of power shifts with different control strategies for the gearbox. Through the structural design of the power shift mechanism control module, the hydraulic power distribution of the hydraulic system of the hydraulic travel module and its control mode are analyzed, and a regional cooperative shift control strategy is proposed in conjunction with control theory. A model of cotton picker dynamics was built using AMESim simulation software. In addition, the traditional control strategy was simulated and compared with the Statement component automatic control strategy to analyze and discuss the control deficiencies in power shift smoothness. Then, a particle swarm genetic algorithm (PSGA) was constructed by integrating the PSO algorithm and the genetic algorithm to verify the effectiveness of the algorithm in improving the dynamic performance and shift smoothness of the gearbox. The algorithm was verified using bench tests, and the algorithm improved the harvesting quality and efficiency of the cotton picker.

Keywords: power shift; shift smoothness; AMESim; PSGA algorithm



Citation: Pan, W.; Wang, L.; Ni, X.; Cai, W.; Zhao, Y.; Chen, H.; Lin, Y.; Zhou, Y. Optimisation of Control Strategies for Power Shift Gearboxes. *Agriculture* **2023**, *13*, 1266. <https://doi.org/10.3390/agriculture13061266>

Academic Editor: Simone Bergonzoli

Received: 16 May 2023

Revised: 13 June 2023

Accepted: 14 June 2023

Published: 19 June 2023



Copyright: © 2023 by the authors. Licensee MDPI, Basel, Switzerland. This article is an open access article distributed under the terms and conditions of the Creative Commons Attribution (CC BY) license (<https://creativecommons.org/licenses/by/4.0/>).

1. Introduction

Cotton pickers work in a harsh environment, with a wide range of working conditions and frequent fluctuations in external loads. To adapt to more demanding operating needs, the gearbox is required to adjust the speed and torque promptly to adapt to the external load and the constant changes in resistance during driving and ensure the power, as well as the fuel economy, of the cotton picker [1–5]. The power shift transmission provides a faster, smoother shifting experience than conventional transmissions. Power shift transmissions have higher efficiency and faster responses than hydrodynamic automatic transmissions [6,7], so studying power shift transmission shift smoothness is crucial.

Most long-term research on transmissions has focused on structure and performance studies [8–11]. With the increasing requirements for smooth gear shifting in transmissions, the advantages and disadvantages of turn control strategies have become a research hotspot. The ISAMO framework was proposed in Study 1 to solve the problem of multi-clutch shifting in automatic transmissions [12]. Study 2 presents a method for optimizing the design of a pressure control valve to improve the stability and response of a clutch actuator system. The method employs experimental design techniques to identify sensitivity in stability boundaries and corresponding output-pressure response times for different parameters. It then applies a particle swarm optimization algorithm for synchronous optimization of the pressure control valve. The experimental results demonstrate significant improvements in the response characteristics and stability performance of the system using the proposed

method [13]. Study 3 addresses the problem of electric vehicle shifting by proposing an optimal shifting schedule and mode selection diagram that integrates a priority factor into the motor efficiency to avoid torque gaps and oscillations [14]. Study 4 presents a control strategy for heavy vehicle shifting, showing how to reduce shift shocks by analyzing the transient shift phenomenon and applying only ten angular velocity signals [15]. Study 5 compares the effectiveness of different shift strategies in a hydromechanical CVT [16]. The new hydraulic–mechanical power return transmission proposed in Study 6 effectively improves system efficiency and reduces oil consumption [17]. In Study 7, fuzzy logic adaptive modifications were used to enhance the performance of pure electric vehicles. The results showed that the two-speed dual-clutch transmission outperformed the single-speed main gearbox [18]. Study 8 describes the design optimization of DCT-HEV's dual-clutch transmission to minimize fuel consumption. The HPSO algorithm is used to solve the optimization problem, obtaining the best gear ratios and shift thresholds under various driving conditions, and resulting in a significant reduction in equivalent fuel consumption [19]. Study 9 investigated methods to improve the switching quality of the wet clutch in agricultural tractors. Through full factorial performance measurement and analysis, the key factors affecting the working quality of the wet clutch, such as oil pressure, flow rate, and load, were determined. In addition, a modeling approach and optimization strategy for adjustable control factors were proposed. In the experiment, oil pressure and flow rate should be adjusted according to the size of the load to reduce sliding friction loss. The results showed that when dynamic load characteristics and speed reduction characteristics were improved, sliding friction loss was also reduced synchronously by up to 70.19%. A total of 225 sets of sample data were obtained using the Simulation X software 2021 simulation platform, and partial least squares and range analysis were used to comprehensively analyze the impact of multiple factors [20].

This article focuses on the power shift gearbox in the 4MZD-6 cotton-packing picking machine as its research subject. We study the gear shift strategy from two perspectives: transmission input characteristics and shift time. The shifting process of a power shift transmission is a complex dynamic process where the clutch undergoes the following phase changes during the shift: the low-gear phase, low-torque phase, inertia phase, and high gear phase. The study of power shift transmission shifting strategy will bring significant challenges to system modeling, simulation analysis, and experimental verification because the smoothness of shifting is related not only to clutch/brake impact and slip-motion work, but also to its input characteristics. This paper first establishes dynamic models of different stages according to the structure of the power shift gearbox, and then, studies the shift strategy under typical operating conditions according to the input characteristics and shift time of the power shift gearbox; finally, it verifies the control strategy through experiments.

2. Materials and Methods

2.1. Power Shift Control Theory

2.1.1. Power shift Control Module

The four-part power shift control module studied in this paper consists of an electronic control module, an electro-hydraulic pilot control valve, a wet clutch/brake, and a transmission system. The drive system of the cotton picker uses a pump-controlled motor to provide torque. It can change the displacement of the hydrostatic pump and motor, as well as control the action of the wet clutch/brake through the movement of the multi-functional control handle to achieve a change in driving speed. In this case, the pump-controlled motor only provides the torque required for low speed, while the switching of low speed to high speed is achieved by the mechanical transmission changing the ratio of the planetary gear structure.

As shown in Figure 1, when the driver performs a shift, the signal is passed to the CAB controller for processing, and then, sends a PWM control signal with different ratios to the electro-hydraulic pilot control valve to control the oil pressure. When the solenoid is energized, the pilot valve spool will be placed correctly. The controlled oil pressure will

push the main valve spool in the left part, and the high-pressure oil flow into the piston chamber will push the piston in the direction of the compression friction plate, making the two drive components in the clutch or brake gradually rotate at the same speed; this enables the clutch or brake to be engaged. Similarly, when the solenoid valve PWM control signal has 0 potential, the piston oil pressure will decrease rapidly, and the disc spring will return to the initial position to complete the separation operation; a multifunctional handle controls the whole process to realize the idling, field transport and road transport of the cotton picker.

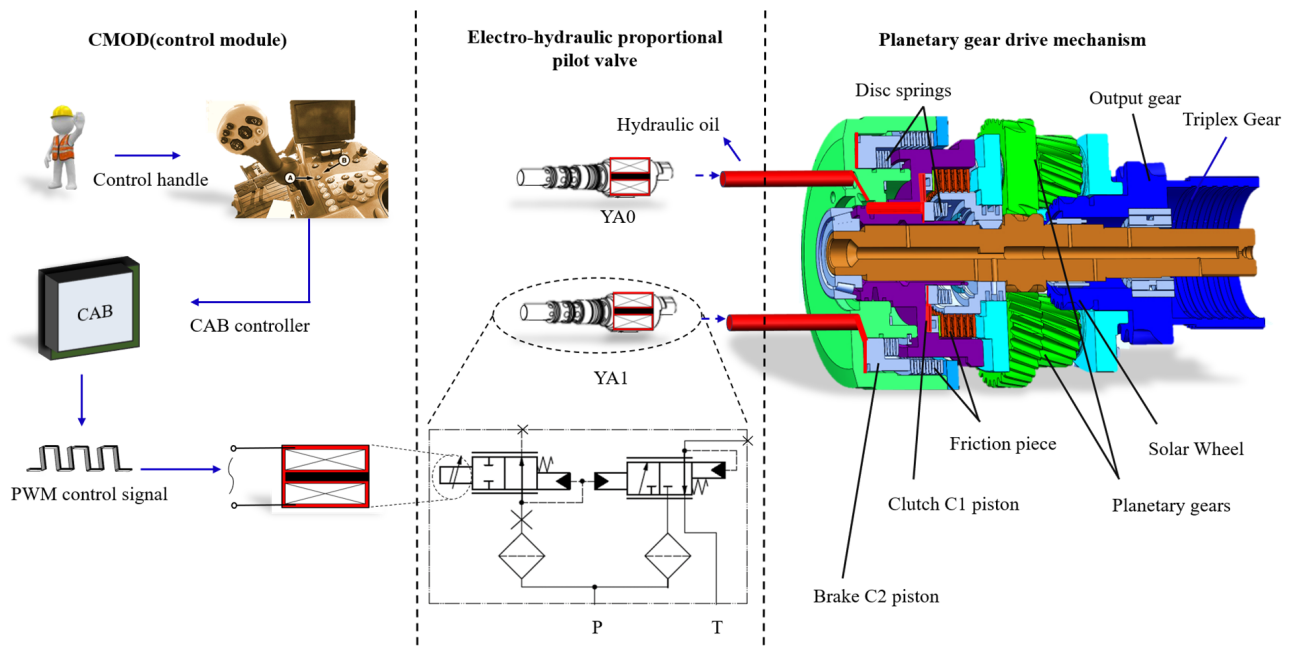


Figure 1. Schematic diagram of the gearshift control module.

2.1.2. Hydraulic Travel System Module

The hydraulic travel system in a cotton picker is composed of variable hydraulic pumps, front and rear-drive variable motors, and hydraulic control elements. The system adjusts the speed and direction of movement by changing the displacement of the variable pump and variable motor, as shown in Figure 2. During field picking work, a small displacement variable pump and large displacement variable motor maintain low-speed and high-torque conditions. In the field and road transport stages, medium and large displacement variable pumps are used, respectively, to accommodate varying speeds. The controller adjusts the motor speed using an electro-hydraulic proportional variable mechanism based on a difference signal between the actual and target speeds of the front- and rear-drive motors. A cross-coupled controller enables real-time monitoring and optimal equalization control of irregular motor operating positions.

2.2. Control Strategy and Whole-Vehicle Model Building

2.2.1. Structure Design of Gearshift Mechanism

The input of the planetary gearshift mechanism is connected to the front-drive variable motor m_1 ; the input shaft is integrated with the sun wheel and transferred to the planetary gear, the planetary gear is fixed to the planetary carrier by its intermediate shaft, and the planetary page and clutch are integrated. In addition, the planetary gear structure is controlled by two wet disc sets of clutch C_1 and brake C_2 . Four states can be obtained using control elements such as pilot proportional solenoid valves (after the actual vehicle verification, the cotton picker works for 1500 h without abnormalities). Table 1 shows the clutch and solenoid valve solenoid action.

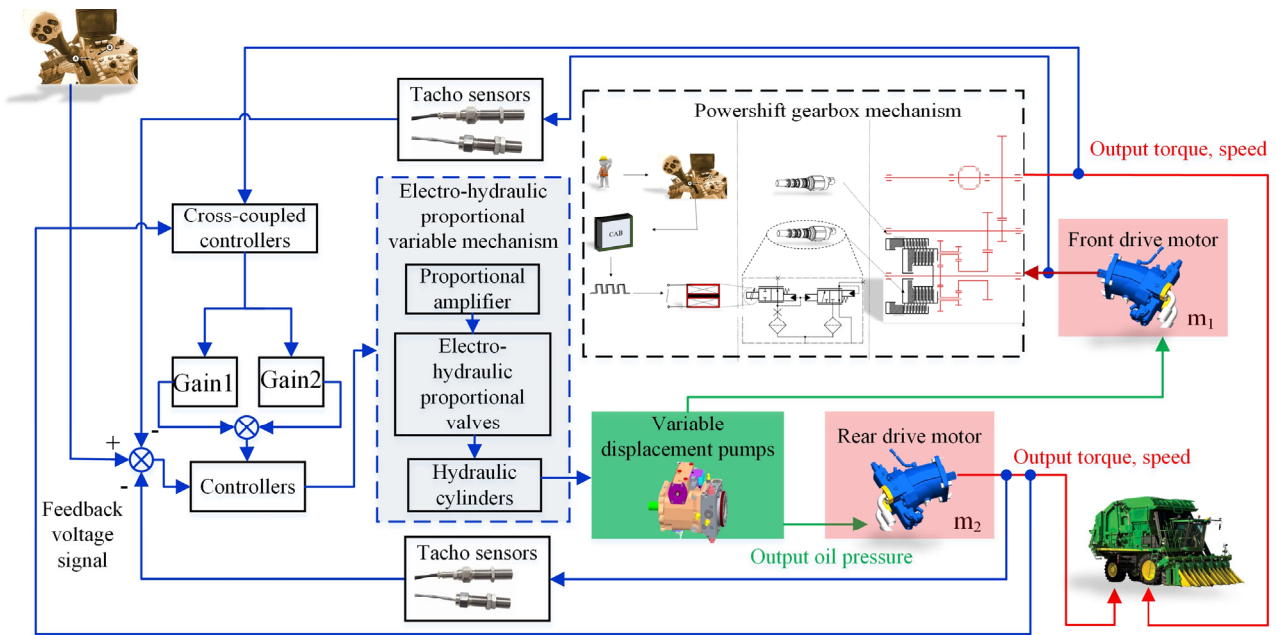


Figure 2. Schematic diagram of the hydraulic travel system module.

Table 1. Clutch and solenoid valve solenoid operation.

Work Conditions	C ₂	C ₁	YA0	YA1
Neutral gear	△	△	△	△
Field Picking	●	△	●	△
Field transportation	●	△	●	△
Road Transportation	△	●	△	●
Braking	●	●	●	●

Note: In the table, YA0 and YA1 represent the solenoid valve in the solenoid core; ● signifies it receives electricity and then it takes action; △ means it does not take action.

2.2.2. Power Shift Speed Ratio Matching

When the cotton picker is in the picking and transport section, the C₂ piston is filled with oil until it is combined. The C₁ piston is returned to the oil, as shown in Figure 3a, and the outer low-speed brake drum is locked to the middle low-speed brake drum. Since the intermediate low-speed brake drum is fixed to the planetary gear frame, the stability of the planetary gear is ensured so that the planetary gear rotates around the input and output sun gear. The output speed is lower than the input speed, and the transmission characteristics are as follows:

$$\omega_{ef} = \frac{\omega_{cd}}{i_{de}} = \frac{\omega_{ab}}{i_{ac}} = \frac{\omega_i}{i_{sb} \cdot i_{ac}} = \frac{\omega_i}{i_{sb} \cdot i_{ac} \cdot i_{de}} \quad (1)$$

$$T_{ef} = -i_{de} \cdot T_{cd} = i_{de} \cdot i_{ac} \cdot T_{ab} = -i_{sb} \cdot i_{de} \cdot i_{ac} \cdot T_i \quad (2)$$

$$n_{ef} = \frac{n_{cd}}{i_{de}} = \frac{n_{ab}}{i_{ac}} = \frac{n_i}{i_{sb} \cdot i_{ac} \cdot i_{de}} \quad (3)$$

where ω_{ef} is the low-speed angular speed of the gearbox, rad/s; ω_{cd} is the low-speed angular speed of the triplex gear, rad/s; ω_{ab} is the low-speed angular velocity of the planetary gear, rad/s; ω_i is the low-speed angular velocity of the solar wheel, rad/s; T_{ef} is the low-speed torque output for the gearbox, Nm; T_{cd} is the low-speed equivalent torque from the planetary pinion to the triplex gear, Nm; T_{ab} is the low-speed equivalent torque between the sun wheel and the big planetary gear, Nm; T_i is the low-speed equivalent

torque from the gearbox input to the sun wheel, Nm; n_{ef} is low-speed gear output for the gearbox, Nm; n_{cd} is the triple gear low speed, r/min; n_{ab} is the planetary gear low speed, r/min; n_i is the low speed of the solar wheel, r/min; i_{sb} is the low-speed ratio between the sun wheel and gear b; i_{ac} is the low-speed ratio between triple gear c and gear a; and i_{de} is the low-speed ratio between triplex gear d and output shaft gear e.

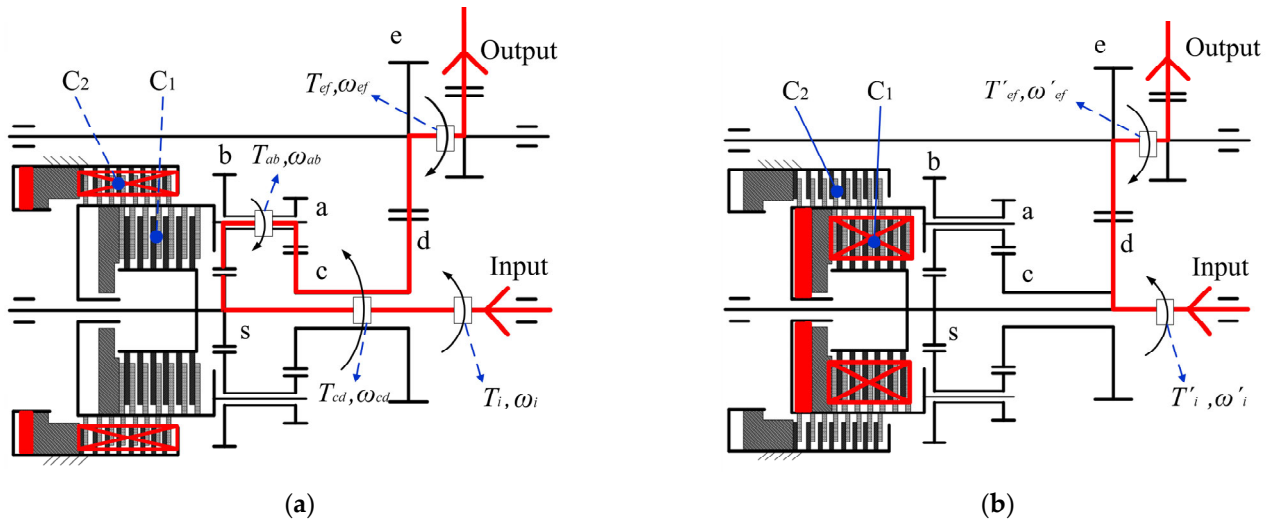


Figure 3. Sketch of power shift mechanism structure. (a) C₂ combined power distribution; (b) C₁ combined power distribution. In the figure, a and b are the two teeth of the duplex gear; c and d are the output teeth and intermediate teeth of the triplex gear; e is the output shaft gear; s is the input sun wheel gear.

When the cotton picker is in the high-speed section of road transport, the C₁ piston is filled with oil until it is combined, and the C₂ piston is returned to the oil; as shown in Figure 3b, the C₁ inner drum is combined with the intermediate drum, and the intermediate drum is rigidly connected to the planetary gear frame, making the input and output speeds equal.

In Figure 3b with the following transmission characteristics:

$$\omega'_{ef} = \frac{\omega'_i}{i_{de}} \tag{4}$$

$$T'_{ef} = -i_{de} \cdot T'_i \tag{5}$$

$$n'_{ef} = \frac{n'_i}{i_{de}} \tag{6}$$

where ω'_{ef} is the high-speed angular speed of the gearbox, rad/s; ω'_i is the high-speed angular velocity of the solar wheel, rad/s; T'_{ef} is the high-speed torque output for the gearboxes, Nm; T'_i is the high-speed equivalent torque from the gearbox input to the sun wheel, Nm; n'_{ef} is the high-speed output speed for the gearbox, r/min; and n'_i is the high speed of the solar rotation, r/min.

The clutch/brake transmission torque is as follows:

$$T_c = \frac{Z\mu'Pd_f s_p}{2} \tag{7}$$

where T_c is the C₁/C₂ transmission torque, Nm; z is the number of friction plates; μ' is the coefficient of the kinetic friction of the friction piece during rotation; P is the C₁/C₂

oil filling pressure, MPa; d_f is the C_1/C_2 average diameter of its friction plate's working surface, mm; and s_p is the C_1/C_2 piston area of action, mm^2 .

2.2.3. Shift Smoothness Rating Index

As the core of the transmission control, the relevant factors for optimization are clutch friction plate slip power, shift shock, clutch binding response speed, etc., which determine the service life and shift smoothness of the clutch and brake. Smooth shifting is mainly achieved by controlling the oil filling characteristics of C_1/C_2 , the manipulation system. In this paper, the friction plate slip work and cotton picker impact of C_1/C_2 are selected as the evaluation indexes of shift smoothness.

Sliding work of friction plate. The meaning of slip work is the work performed by the friction plate and steel plate in the clutch/brake during the individual bonding process, i.e., the magnitude of the work performed by the friction torque, the mathematical expression of which is:

$$W = \int_{t_{ps}}^{t_1} T_C(\omega_1 - \omega_2) dt \tag{8}$$

where t_1 is end of the shift moment, s; t_{ps} is the initial moment of gear change, s; T_C is the C_1/C_2 transmission torque, Nm; ω_1 and ω_2 are the active and passive friction plate angular velocity of C_1/C_2 , rad/s.

Shift shock. Shock is an indicator of the rate of change of the vehicle's longitudinal acceleration, and is closely related to the rate of change of the torque of the engagement element. It reflects the torque fluctuation of the transmission output shaft when shifting, and is an important indicator of the smoothness of the shifting process. The German standard maximum shock degree for $j = 10 \text{ m/s}^3$.

$$j = \frac{da}{dt} = \frac{d^2v}{dt^2} \tag{9}$$

where j is the shift impact degree, m/s^3 ; a is the longitudinal acceleration of the cotton picker, m/s^2 ; and v is the driving speed of the cotton picker, km/h.

2.2.4. Power Upshift Process Analysis

Cotton pickers and other construction vehicles are generally divided into four types of shift process: power upshift, power down-shift, un-power up-shift, and un-power down-shift, where the power upshifts when the cotton picker engine outputs torque to provide the full vehicle with drive torque in the vehicle acceleration process of upshifting [21–24].

As shown in Figure 4, the power upshift process can be divided into four phases, namely, the low-gear phase, the low-gear torque phase, the inertia phase, and the new-gear phase:

Low-gear stage. We set a t_{ps} moment as the power shift point. The CAB controller issues a signal, and the solenoid valve quickly responds. Regarding the C_1 and C_2 control valves, at the exact moment of receiving the password, the C_1 piston begins to fill with oil, and at this time, its friction plate and steel sheet are not combined, so it cannot transfer torque; the C_2 piston is still in a high-pressure state, its friction plate and steel sheet maintain their pressure state, and the transmission torque does not change. At this stage, the power shift mechanism output characteristics are:

$$\begin{cases} T_{C_1} = 0 \\ T_{C_2} = \frac{z_2 \mu' P_2 d_{fC_2} s_{pC_2}}{2} \end{cases} \tag{10}$$

where T_{C_1} is the C_1 transmission torque, Nm; z_2 is the number of C_2 friction plates; P_2 is the C_2 oil filling pressure, MPa; d_{fC_2} is the average diameter of the C_2 friction plate's working surface, mm; and s_{pC_2} is the C_2 piston action area, mm^2 .

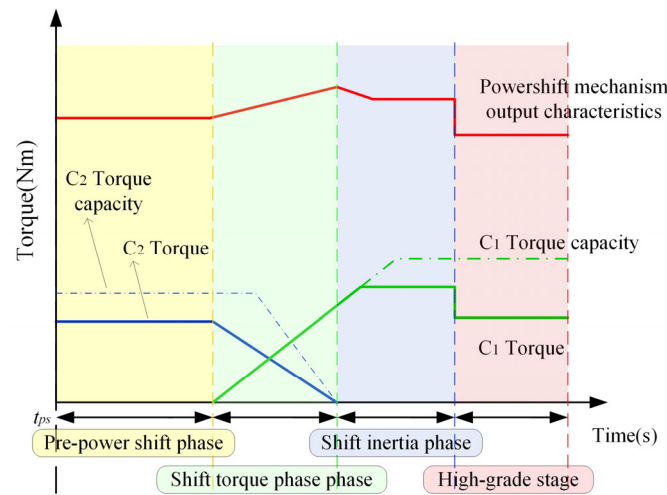


Figure 4. Power distribution when the brake and clutch are combined.

Low-gear torque phase. At this time, the C_2 piston oil pressure begins to fall. At this time, the C_2 piston oil pressure begins to decrease, but the C_2 friction plate and steel plate are still in the engaged state. When the engaging C_1 piston oil pressure starts to rise and enters the slipping state, the friction plate and steel plate transfer a portion of the torque moment. The output characteristics of the power shift mechanism are as follows:

$$\begin{cases} T_{c1} = \text{sign}(\omega_1 - \omega_2)\mu' s_{pc1} P_{n1} z_1 \frac{2}{3} \left(\frac{R_{01}^3 - R_{11}^3}{R_{01}^2 - R_{11}^2} \right) \\ T_{c2} = \frac{z_2 \mu' P_2 d_{f2} s_{pc2}}{2} \end{cases} \quad (11)$$

where sign represents the symbolic functions.

$$\text{sign}(\omega_1 - \omega_2) = \begin{cases} 1 & \omega_1 - \omega_2 \geq 0 \\ -1 & \omega_1 - \omega_2 < 0 \end{cases} \quad (12)$$

where s_{pc1} is the C_1 piston action area, mm^2 ; P_{n1} is the C_1 operation, the piston unit area action pressure, MPa; z_1 is the number of C_1 friction plates; and R_{01} and R_{11} are the C_1 inner diameter and outer diameter, respectively, mm.

Inertial phase. The C_2 piston oil pressure decreases so that its transmission torque decreases and enters the inertia phase, C_1 , to be combined. It is in the slip-motor state, and its friction plate and steel plate transmit part of the torque. The output characteristics of the power shift mechanism are:

$$\begin{cases} T_{c1} = \text{sign}(\omega_1 - \omega_2)\mu' s_{pc1} P_{n1} z_1 \frac{2}{3} \left(\frac{R_{01}^3 - R_{11}^3}{R_{01}^2 - R_{11}^2} \right) \\ T_{c2} = \text{sign}(\omega_1 - \omega_2)\mu' s_{pc2} P_{n2} z_2 \frac{2}{3} \left(\frac{R_{02}^3 - R_{12}^3}{R_{02}^2 - R_{12}^2} \right) \end{cases} \quad (13)$$

where P_{n2} is the C_2 operation, the piston unit area action pressure, MPa; z_2 is the number of C_2 friction plates; and R_{02} and R_{12} are the C_2 inner diameter and outer diameter, respectively, mm.

High-grade stage. The oil pressure of the C_2 piston drops until it stops sliding and separates. At the same time, C_1 begins sliding with the increase in oil pressure. The angular velocity ω_1 and ω_2 between the driving and driven discs is the same until it gradually reaches $T_{C1} = 0$. Each component satisfies the following:

$$\frac{d\omega}{dt} = 0 \quad (14)$$

where ω is the angular velocity of each component.

2.2.5. Shift Control Strategy

Based on the power shift control system analysis above, a shift control strategy, as shown in Figures 5 and 6, is proposed, with dual-zone power shift transmission with a low speed-to-high speed power shift used as an example in this paper.

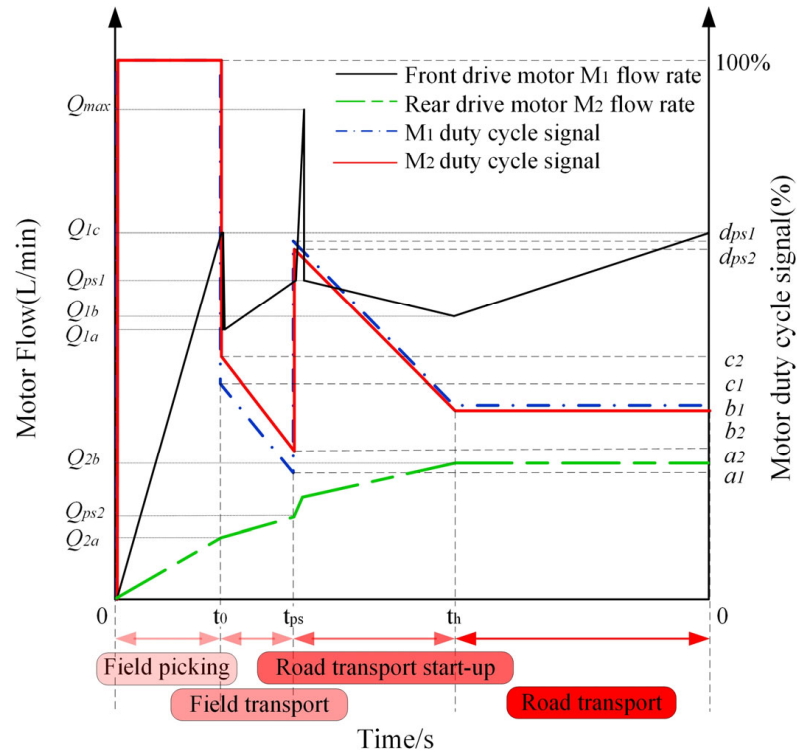


Figure 5. Variable motor partition section control strategy.

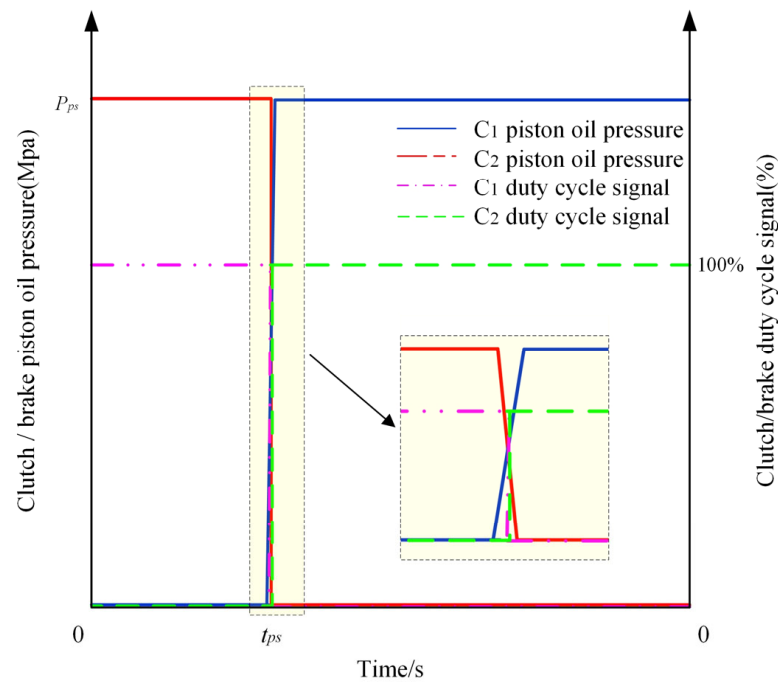


Figure 6. C1C2 partition segment control strategy.

To accelerate the vehicle at low speeds, the pump displacement must be increased to 100%, keeping both motor displacements at 100%. Then, the engine speed is constant, so the flow rate in the system is conserved; so, to increase the vehicle speed (and the hydraulic motor speed), the displacement of the hydraulic motor must be reduced (in the medium speed phase).

Due to the unsatisfactory efficiency of the motor, small displacements should be avoided. Therefore, the transmission ratio is constantly changed using clutch C_1 /brake C_2 while keeping the motor displacement above a too-low value (here, 35%). The regional cross-shift control strategy proposed in this paper is divided into four stages:

Low-speed stage (0~ t_0). At this stage, the pump, front-drive variable motor m_1 , and rear-drive variable motor m_2 all reach 100% displacement hold, allowing the vehicle to obtain high-torque low-speed running capability at start-up; the C_1 electro-hydraulic pilot control valve duty cycle signal is 100%, the C_2 electro-hydraulic pilot control valve duty cycle signal is 0%, and the status is held until the vehicle speed is V_1 .

Medium-speed stage (t_0 ~ t_{ps}). At t_0 , the moment of the vehicle speeds up to V_1 , at the exact moment of the m_1 and m_2 duty cycle signals produced by c_1 and c_2 , respectively, which are converted to a_1 and a_2 . The electro-hydraulic pilot control valve duty cycle signals of C_1 and C_2 are maintained at 100% and 0% until the vehicle speed is V_m .

High-speed stage (t_{ps} ~ t_h). At t_{ps} , the moment of the car speeds up to V_m . In order to achieve a higher speed output and power shift, the electronic control module issues a PWM signal, controlling the C_1 and C_2 electro-hydraulic pilot control valve, clutch, and brake action at the same time. The duty cycle signal undergoes a power shift from 100% and 0% to 0% and 100%, while the duty cycle signals of motors m_1 and m_2 from a_1 and a_2 bail up to d_{ps1} and d_{ps2} in a transmission ratio change, until the car speed is V_h .

Road driving stage (t_h ~). At t_h , the moment of the vehicle speeds up to V_h , so that the cotton picker moves at the highest uniform speed.

2.3. AMESim Model Building

Using AMESim (2021) software as a tool, a closed-loop hydraulic system control model was established, and two relief valves, a flushing valve, and a charge pump with a check valve were used for simulation and analysis. In addition, the performance and characteristic parameters of the power shift hydraulic transmission system of the cotton picker were verified, as shown in Figure 7.

To obtain the ideal signals for the hydraulic control system and C_1 and C_2 , the Statechart component automatic control model was built in AMESim software based on the above control strategy, as shown in Figure 8. It enables the calculation of each stage's output, considering the transmission ratio. In the high-speed location, the output of the variable motor is as follows:

$$m_1 = m_2 = pump_{cc} V_{eff} \frac{\omega_{target}}{V_{target} \left(\frac{m_{1cc}}{r_{atio1}} + \frac{m_{2cc}}{r_{atio2}} \right)} \quad (15)$$

where ω_{target} is the target engine speed, rad/s; V_{target} is the target speed of the cotton picker, km/h; $pump_{cc}$ is the maximum displacement of the pump, mL/r; m_{1cc} is the maximum displacement of the front-drive variable motor, mL/r; m_{2cc} is the maximum displacement of the rear-drive variable motor, mL/r; V_{eff} is the volumetric efficiency, %; r_{atio1} is the ratio between the front-drive variable motor and the wheel; and r_{atio2} is the ratio between the rear-drive variable motor and the wheel, mL/r.

The parameter values used in the AMESim simulation tests were mainly determined based on the structural parameters of the hydraulic system. In contrast, the parameters affected by the control strategy were derived from multiple structure simulations. The main parameters are shown in Table 2. Using the AMESim complete machine model illustrated above, we set the simulation time to 40 s and the step to 0.01.

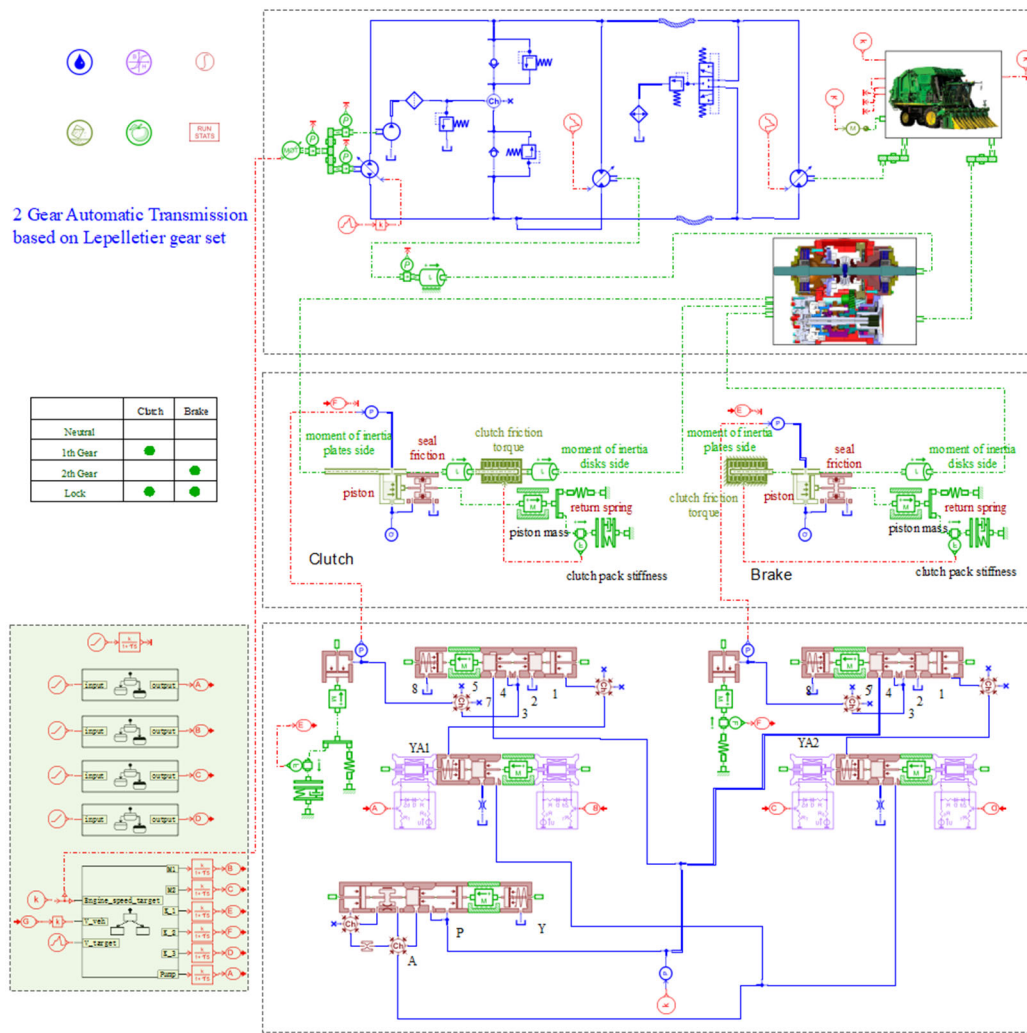


Figure 7. AMESim whole-vehicle model construction.

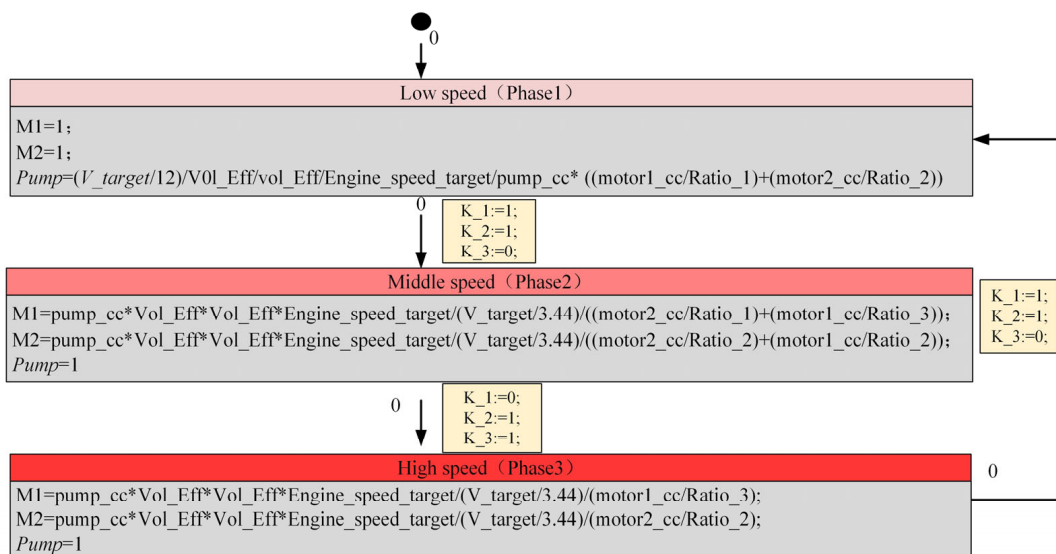
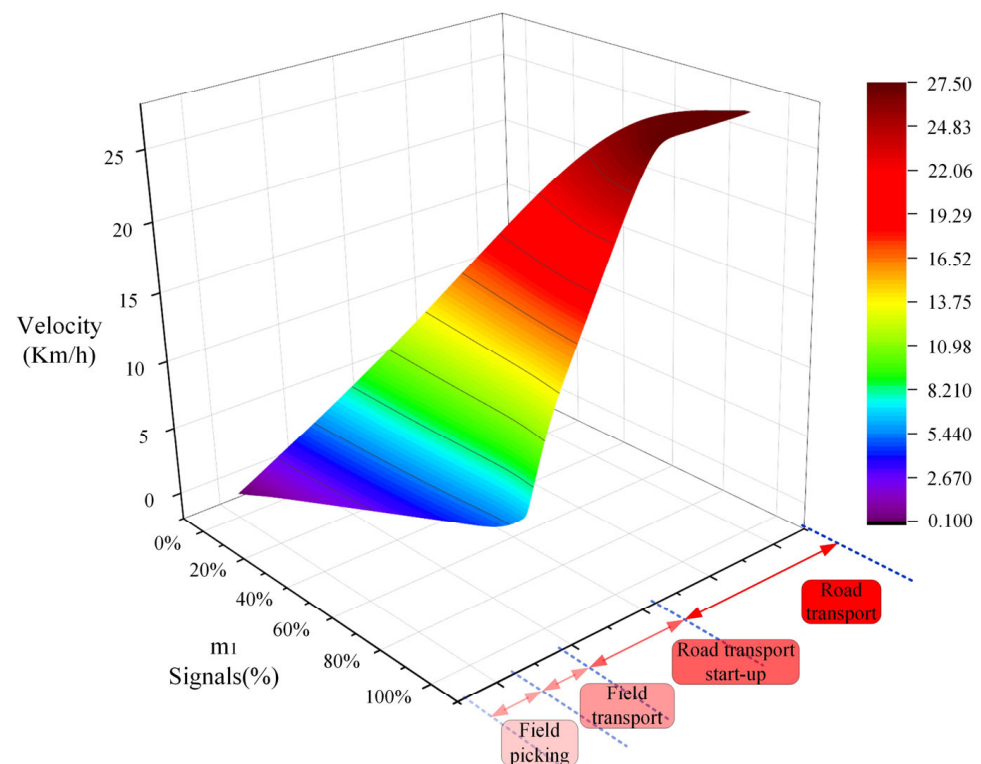


Figure 8. Statechart component.

Table 2. Shift control parameters.

Name	Value	Name	Value
a_1	23.3%	b_2	35%
a_2	27.1%	d_{ps1}	66.6%
b_1	36%	d_{ps2}	64.8%

Figure 9 shows the response of the vehicle speed and the variable motor (m_1) control signal for the cotton picker under different operating conditions. It can be seen from the figure that, under the control of the Statechart component automatic control model, the maximum driving speed of the cotton picker reached 27.52 km/h, and the speed of the car steadily increased under different working conditions. The speed of the cotton picker can reach 7.52 km/h when picking in the field, and when transporting in the area, the driving speed can reach 14.53 km/h. It should be noted that there is a non-linear relationship between the driving speed and the control signal of the variable motor (m_1); this means that the driving speed does not change proportionally to the control signal; this is due to the change in speed of the cotton picker during the change in the control signal of the variable motor (m_1) with a change in the throttle pedal opening.

**Figure 9.** Travel speed of cotton pickers in each section.

In Figure 10, we can see the effect of the power upshift between the conventional control strategy and the Statechart component control strategy during the operation of the cotton picker under the same operating conditions. A number of parameter data were collected after the simulation, including cotton picker driving speed, C_1 and C_2 piston oil pressure, transmission output torque, and shift shock, and were compared and analyzed in detail.

Regarding the C_1 piston oil pressure response, we can see that the conventional control takes 0.45 s to raise the C_1 piston oil pressure to a maximum of 3 MPa. The Statechart component control takes only 0.34 s, a 32.3% faster response time, and the entire gearshift process is much quicker. In addition, for the C_2 piston oil pressure, the conventional

control takes 0.63 s to reduce to low pressure (0 MPa). In comparison, the Statechart component control takes in 0.59 s, which shortens the response time by 6.7% compared to the conventional control.

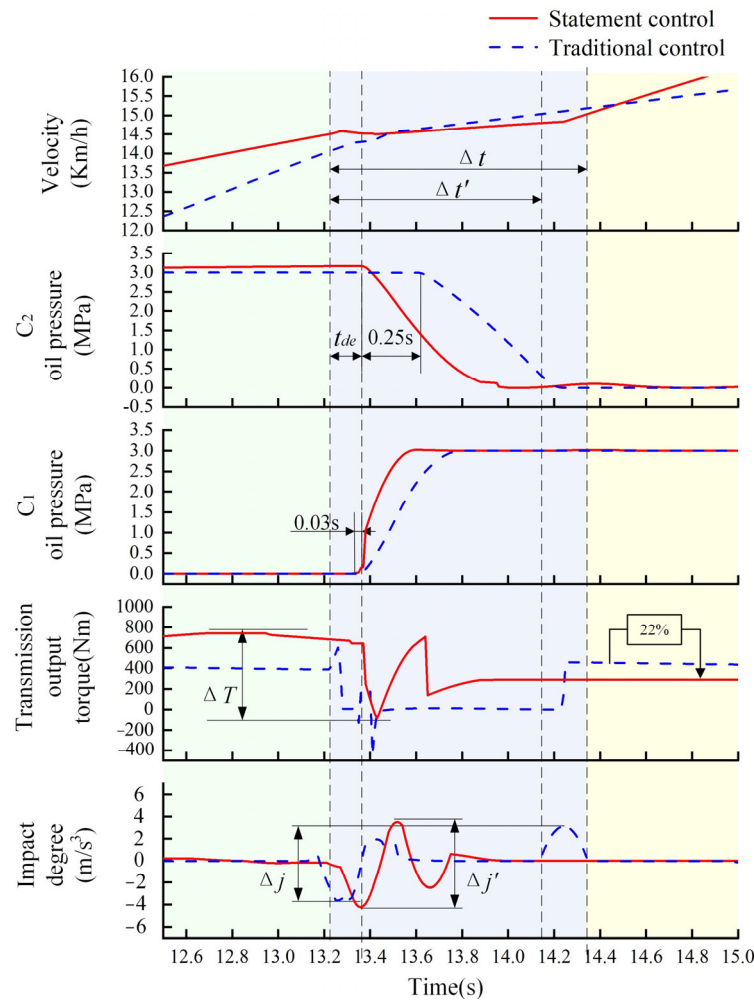


Figure 10. Power shift simulation curve before and after Statechart component control.

Regarding the transmission shift signal response speed, from the simulation results, we can see that the CBA controller sends a signal at 13.21 s after both control strategies undergo hysteresis, and the Statechart component control in C_1 is 0.03 s ahead of the conventional control, meaning they are basically the same. The Statechart component control in C_2 overrides the conventional control by 0.25 s. However, the Statechart component control is significantly better than the conventional control; its response speed is improved by 23.07% and 62.5%, respectively, enabling faster vehicle shifting.

In the absolute response curve of the transmission output torque float, we can see that the conventional control exhibits greater instability and oscillation. The Statechart component control has better stability and robustness and can better control the variable motor to improve the control accuracy of the whole system. Specific data show that the Statechart component control is 22% lower than the conventional control, and the final output torque is reduced to about 389 Nm.

In this experiment, the sum of the peak absolute values of shift impact using the Statechart component control is 7.6 m/s^3 , an increase of 23.68% compared to 5.8 m/s^3 in the conventional control. This is due to the increased shift shock caused by the shortened shift time under the Statechart component control. However, there is a contradiction between different evaluation indexes regarding the smoothness of gear shifts. For example, too fast a clutch/brake combination time will reduce slip work but increase shift shock; conversely, if

the bonding time is too slow, it will increase the slip work but reduce the shift impact. At the same time, excessive frictional work of the clutch/brake will lead to increased power loss and may make the output torque insufficient to overcome the resistance torque. In addition, if there are large oscillations in the transmission output torque, the shock level may also be higher. When designing a transmission control system, different factors need to be taken into account to optimize the smoothness of shifts. Specifically, the control of clutch/brake combination time, friction coefficient, and output torque needs to be optimized to achieve linear acceleration and smooth shifting.

In summary, it is clear that the Statechart component control strategy developed above is practical. However, the parameters set by the simulation are not optimal, and there is still a lack of control over the smoothness of power shifts. Therefore, based on the proposed Statechart component control strategy, the optimization of model parameters based on the combination of the genetic algorithm and particle swarm algorithm will be presented to improve the power shift smoothness.

2.4. Model Parameter Optimization and Analysis

This paper proposes a particle swarm genetic algorithm (PSGA) for multi-objective optimization when multiple parameters are involved. The PSGA algorithm combines a particle swarm optimization algorithm with a genetic algorithm using the embedded approach, combining the advantages of both algorithms, avoiding the disadvantage of the PSO algorithm tending to fall into local optimum; this effectively improves the algorithm's optimization search [25–28].

2.4.1. Optimization Variable Selection

According to the above shift control strategy, the brake and clutch act simultaneously for upshifting, the clutch C_1 and brake C_2 combination time plays a crucial role in the smoothness of the power shift, and C_1 and C_2 combined with time Δt_1 and Δt_2 are selected as optimization variables; in addition, the clutch C_1 binding oil pressure P_{C1} affects the slip-motion work produced by the clutch plate. It is also used as an optimization variable. The search space of the particle swarm genetic algorithm corresponding to the three selected optimization variables is a three-dimensional 3D space, and the particles are all 3D vectors.

2.4.2. Constraint Establishment

Regarding the AMESim entire-vehicle simulation test, since none of the power shift times exceed 1 s, and considering there is no action before C_1 binding, the upper limit of Δt_1 was set within 1 s and Δt_2 was set to 0.8 s. The lower limit of time in reference [29] is 0.1 s, and combined with the simulation test, in this paper, the lower limits were set to 0.2 s and 0.4 s, respectively, and the PC1 interval was set to (1.5–3) MPa.

In summary, the search space of the particle swarm genetic algorithm for power shift simulation can be expressed as:

$$x_i^t = \begin{bmatrix} 0.2, 1 \\ 0.4, 0.8 \\ 1.5, 3 \end{bmatrix}$$

2.4.3. Objective Function Establishment

Consider the impact of all target indicators to achieve a balance between the different objectives. According to the optimization objective, we can apply the multi-objective particle swarm genetic algorithm to establish an objective equation to solve the dynamics problem [30,31]. First, define the objective of the problem: reducing the shock, sliding work, and transmission input torque oscillation amplitude (variable motor m1 output torque).

To optimize all objectives, they need to be weighted to obtain the weighted objective equation:

$$F(x) = w_1 f_1(x) + w_2 f_2(x) + w_3 f_3(x)$$

where, w_1 , w_2 , and w_3 are the weighting factor for these objectives, $f_1(x)$, $f_2(x)$, and $f_3(x)$ are functions of the state variables for shock degree, slip work, and torque.

Using a multi-objective particle swarm genetic algorithm, optimization can be performed on different objective functions to satisfy the above three objectives simultaneously. After reaching equilibrium, the set of optimal keys can be obtained, where each solution is optimal and non-dominated for all objectives [32,33].

2.4.4. Analysis of Simulation Results

We edited the multi-objective particle swarm genetic algorithm-based program in Matlab (2021-b) software. A nonlinear regression equation was derived from the simulation curves in Section 2 and substituted into the algorithm program for simulation optimization, and the simulation parameters were set as in Table 3, the algorithmic objective function adaptation of the optimization process is shown in Figure 11, after the optimization of the algorithm, it can be seen that it starts to converge after the 49th iteration, the optimal solution is 0.3266, $\Delta t_1 = 0.7533$ s, $\Delta t_2 = 0.5315$ s, $P_{C1} = 2.8912$ MPa.

Table 3. Parameters of multi-objective particle swarm genetic algorithm.

Parameters	Maximum Number of Iterations	Number of Initial Particle Groups	w_1	w_2	w_3
Value	100	100	2	2	2

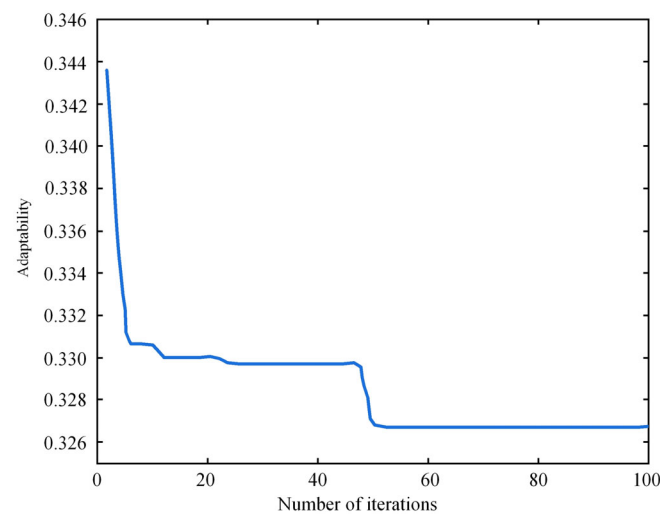


Figure 11. Particle swarm genetic algorithm adaptation curve.

We substituted the optimal solution into the AMESim model. The parameters obtained after the simulation are shown in Table 4. The slip work after particle swarm genetic optimization is 1215.9 J, and the reduction is 8.0% and 14.6% compared to the Statechart component control strategy and the conventional control strategy, respectively. The optimized impact degree is 5.21 m/s³, which is 31.4% and 10.1% lower than the Statechart component control strategy and the conventional control strategy, respectively. The absolute value of the output torque amplitude of the variable motor m1 is optimized to be 893.3 Nm, which is 6.4% and 14.2% less than the Statechart component control strategy and the conventional control strategy, respectively. A data comparison curve of the cotton picker traveling speed simulation optimization is shown in Figure 12. After optimization, the response time to reach the target vehicle speed is advanced by 2.67 s. Due to the reduction in slip-motor work, the shift time is correspondingly reduced. As can be seen from the partial magnification, the vehicle speed oscillates at all power shift points, and the vehicle speed increases by 0.21 s compared with the power shift time before optimization, and the integrated shift smoothness is optimized by 18.3% after optimization.

Table 4. Comparison of evaluation indicators after optimization.

Objectives	Traditional	Statechart Component	Particle Swarm Genetic Optimization	Target Changes
W (J)	1423.2	1321.5	1215.9	↓
J (m/s^3)	5.8	7.6	5.21	↓
ΔT (Nm)	1033	954.2	893.3	↓

Note: ↓ representative decline.

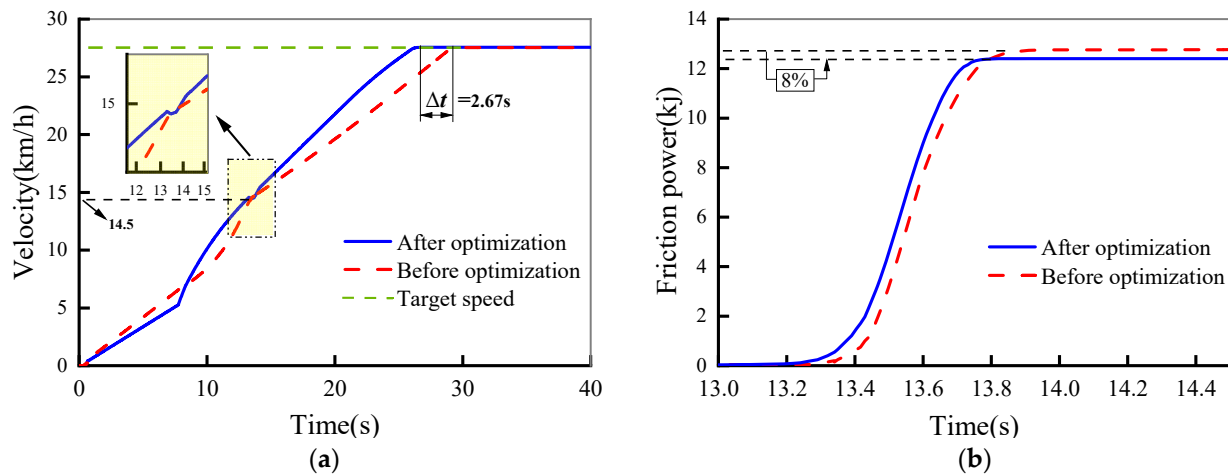


Figure 12. Particle swarm optimization curve. (a) C_2 oil pressure change curve; (b) C_1 oil pressure change curve.

3. Bench Test Verification

3.1. Test Stands

The experimental test setup is shown in Figure 13a, and the real test rig is shown in Figure 13b. A 250 mL/r displacement variable pump provides flow to a 160 mL/r displacement variable motor, which then provides power to the gearbox via the motor. In addition, a brake matching the gearbox is installed at the output shaft of the power shift gearbox, torque speed sensors are installed on each side of the two brakes, and the rest of the sensors are lined up on the variable pump, variable motor, gearbox, and other devices being tested.

3.2. Test Results

Figure 14 shows a comparison between the test and simulation of the C_1 and C_2 pressure responses under the optimized parameters of the particle swarm algorithm. In Figure 14a, the C_2 oil pressure response time is 0.09 s ahead of the simulation, and the switching process lasts 0.63 s, which is 13% less than the simulation time, and the oil pressure finally drops to 0.18 MPa. This is because the C_2 hydraulic control valve oil port is not completely closed, and there is a discrepancy with the simulation. In Figure 14b, the C_1 oil pressure response lags by 0.07 s compared with the simulation, and the switching process lasts 0.52 s, which is 5% less than the simulation time. The pressure overshoot is more significant than the simulation. After comparing the test and simulation, it is found that the test results indicate that the oil pressure stability was relatively poor. Upon further analysis, it is found that there was a discrepancy between the experimental and simulation results. Additionally, the difference is due to the influence of valve clearance leakage. The simulation model did not consider the influence of valve gap leakage, resulting in low experimental results. In addition, hydraulic line leakage was also considered, and the results show that the experimental oil pressure was slightly lower than the simulated oil pressure.

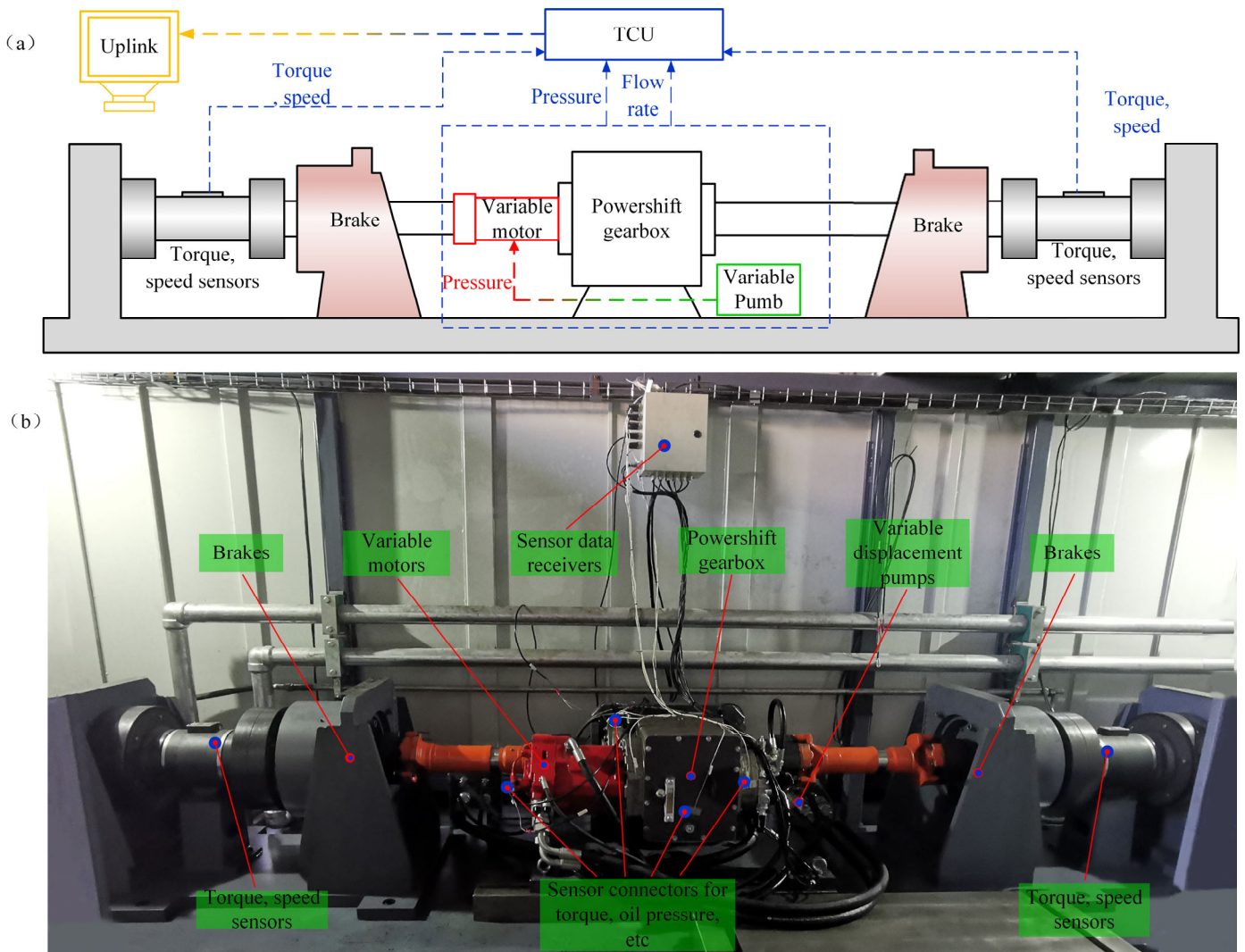


Figure 13. Schematic diagram of the test stand. The experimental test setup is shown in (a), the real test bench is shown in (b).

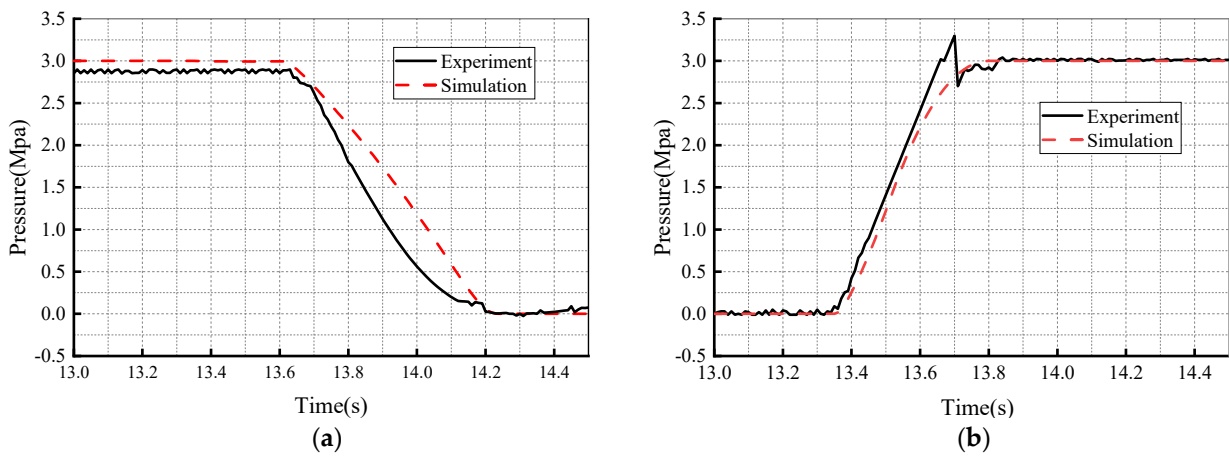


Figure 14. Experimental and simulation results of pressure response. (a) C_2 oil pressure change curve; (b) C_1 oil pressure change curve.

Figure 15a shows the change curve of the output torque of the variable motor during the power shift, and the comparison analysis shows that the response time of the torque

curve derived from the test is 0.06 s ahead of the simulation time. Nevertheless, Figure 15b shows a large amplitude of the impact degree variation curve, whose highest value reaches 5.6 m/s^3 , which is 30.2% higher than the simulation. Essentially, the simulated curves show good agreement with the experimental results. However, the consistency of the test and simulation result trends is poor, and the oscillation amplitude is large, which is due to the high temperature of the hydraulic fluid in the test system; when the temperature increases, the viscosity of the hydraulic fluid decreases, resulting in increased oscillation of the shift shock (the temperature fluctuation range of hydraulic oil was tested to be 0–88 degrees Celsius). These findings suggest that we need to set and adjust the model details and parameters more accurately in order to further validate the simulation data.

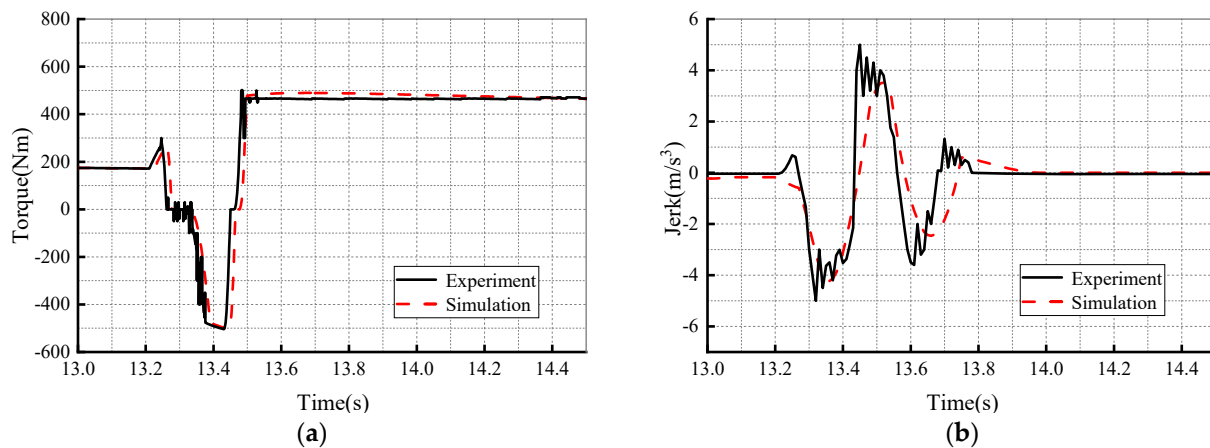


Figure 15. Test data and optimization data. (a) m_1 output torque curve; (b) impact change curve.

4. Conclusions

(1) This paper takes the power shift gearbox of a cotton picker as the research object, explores the influence of the power shift gearbox on the performance of a cotton picker, develops a power distribution diagram of the gearshift mechanism, and analyzes the transmission characteristics. On this basis, the power upshift process is analyzed, the output characteristics of each stage of the upshift process are analyzed, a regional coordinated shift control strategy is proposed, and control of the whole cotton picker is carried out.

(2) Based on the above control strategy, AMESim models the whole vehicle, including the shift mechanism control module, the hydraulic travel module, and the control signal module. In addition, in order to obtain the ideal signals of a hydraulic control system and C_1 and C_2 , based on the above control strategy, the Statechart component automatic control model is built in AMESim to simulate, compare, and analyze the traditional control signal via the Statechart component control strategy, to verify the regional cross-shift control strategy and determine the driving speed of the cotton picker, C_1 and C_2 piston oil pressure, transmission output torque, and shift shock variation curves. The Statement control is better than the traditional control, the response speed is relatively increased, by 23.07% and 62.5%, respectively, and the transmission input torque floating absolute value is reduced by 22%.

(3) The absolute value of the difference in shock magnitude under Statement control is relatively higher, by 23.68%, and the shift shock increases. In this paper, the advantages of the PSO algorithm and genetic algorithm are combined, and the disadvantages of the PSO algorithm are improved. An embedded method is used to combine the particle swarm algorithm and genetic algorithm to form a particle swarm genetic algorithm (PSGA), and multi-objective optimization is performed in Matlab to determine the shift impact degree, slip friction work, and transmission input torque.

(4) The final research results obtained through bench test verification show that the PSGA optimization algorithm can effectively improve the dynamic performance and shift smoothness of the gearbox, and improve harvesting quality and work efficiency.

Author Contributions: Conceptualization, W.P., L.W. and W.C.; methodology, X.N.; software, W.P.; validation, W.P., H.C., W.C. and Y.Z. (Yongqiang Zhao); formal analysis, W.C.; investigation, X.N.; resources, L.W.; data curation, Y.Z. (Yuhan Zhou) and Y.L.; writing—original draft preparation, W.P.; writing—review and editing, W.P.; visualization, X.N.; supervision, L.W.; project administration, L.W.; funding acquisition, X.N. All authors have read and agreed to the published version of the manuscript.

Funding: This research was supported by grants from the National Natural Science Foundation of China (Grant No. 2022AA001).

Institutional Review Board Statement: Not applicable.

Data Availability Statement: All relevant data presented in this article are kept at the request of the institution and are therefore not available online. However, all data used in this manuscript are available from the corresponding authors.

Conflicts of Interest: The authors declare no conflict of interest.

References

- Kulkarni, M.; Shim, T.; Zhang, Y. Shift dynamics and control of dual-clutch transmissions. *Mech. Mach. Theory* **2007**, *42*, 168–182. [[CrossRef](#)]
- Dua, R.; White, K.J.; Lindland, R. Understanding Potential for Battery Electric Vehicle Adoption Using Large-Scale Consumer Profile Data. In Proceedings of the Transportation Research Board 96th Annual Meeting, Washington, DC, USA, 8–12 January 2017.
- Boulanger, A.G.; Chu, A.C.; Maxx, S.; Waltz, D.L. Vehicle Electrification: Status and Issues. *Proc. IEEE* **2011**, *99*, 1116–1138. [[CrossRef](#)]
- Hu, X.; Martinez, C.M.; Yang, Y. Charging, power management, and battery degradation mitigation in plug-in hybrid electric vehicles: A unified cost-optimal approach. *Mech. Syst. Signal Process.* **2017**, *87*, 4–16. [[CrossRef](#)]
- Liu, Y.; Li, J.; Chen, Z.; Qin, D.; Zhang, Y. Research on a multi-objective hierarchical prediction energy management strategy for range extended fuel cell vehicles. *J. Power Sources* **2019**, *429*, 55–66. [[CrossRef](#)]
- Ye, J.; Huang, X.; Zhao, K.; Liu, Y. Optimal coordinating control for the overlapping shift of a seamless 2-speed transmission equipped in an electric vehicle. *Proc. Inst. Mech. Eng. Part I J. Syst. Control Eng.* **2017**, *231*, 095965181773017. [[CrossRef](#)]
- Xu, G.; Xu, K.; Zheng, C.; Zhang, X.; Zahid, T. Fully Electrified Regenerative Braking Control for Deep Energy Recovery and Maintaining Safety of Electric Vehicles. *IEEE Trans. Veh. Technol.* **2015**, *65*, 1186–1198. [[CrossRef](#)]
- Linares, P.; Méndez, V.; Catalán, H. Design parameters for continuously variable power-split transmissions using planetaries with 3 active shafts. *J. Terramech.* **2010**, *47*, 323–335. [[CrossRef](#)]
- Gupta, A.K.; Ramanarayanan, C.P. Analysis of circulating power within hybrid electric vehicle transmissions. *Mech. Mach. Theory* **2013**, *64*, 131–143. [[CrossRef](#)]
- Ramdan, M.I. Optimal Design of a Hydro-Mechanical Transmission Power Split Hybrid Hydraulic Bus. Ph.D. Thesis, University of Minnesota, Minneapolis, MN, USA, 2013.
- Macor, A.; Rossetti, A. Optimization of hydro-mechanical power split transmissions. *Mech. Mach. Theory* **2011**, *46*, 1901–1919. [[CrossRef](#)]
- Wang, F.W.Y.; Han, J.; Yao, J. Experimental-wAG-shifttransmission. *J. Cent. South Univ. Engl. Ed.* **2017**, *24*, 7.
- Jian, H.; Wei, W.; Li, H.; Yan, Q. Optimization of a pressure control valve for high power automatic transmission considering stability. *Mech. Syst. Signal Process.* **2018**, *101*, 182–196. [[CrossRef](#)]
- Cong, T.; Pdw, A.; Nong, Z. Optimization and coordinated control of gear shift and mode transition for a dual-motor electric vehicle—ScienceDirect. *Mech. Syst. Signal Process.* **2021**, *158*, 107731.
- Meng, F.; Tao, G.; Chen, H. Smooth shift control of an automatic transmission for heavy-duty vehicles. *Neurocomputing* **2015**, *159*, 197–206. [[CrossRef](#)]
- Zhu, Z.; Gao, X.; Cao, L.; Cai, Y.; Pan, D. Research on the shift strategy of HMCVT based on the physical parameters and shift time. *Appl. Math. Model.* **2016**, *40*, 6889–6907. [[CrossRef](#)]
- You, Y.; Sun, D.; Qin, D.; Wu, B.; Feng, J. A new continuously variable transmission system parameters matching and optimization based on wheel loader. *Mech. Mach. Theory* **2020**, *150*, 103876. [[CrossRef](#)]
- He, B.C.; Chen, Y.; Wei, Q.; Wang, C.; Wei, C.; Li, X. Performance Comparison of Pure Electric Vehicles with Two-Speed Transmission and Adaptive Gear Shifting Strategy Design. *Energies* **2023**, *16*, 3007. [[CrossRef](#)]
- Cao, X.; Du, C.; Yan, F.; Xu, H.; Sui, Y. Parameter Optimization of Dual Clutch Transmission for an Axle-split Hybrid Electric Vehicle. *IFAC Pap.* **2019**, *52*, 423–430. [[CrossRef](#)]
- Yu, C.Y.C.Z.Q. Research on wet clutch switching quality in the shifting stage of an agricultural tractor transmission system. *Agriculture* **2022**, *12*, 1174.
- Qi, X.; Yang, Y.; Wang, X.; Zhu, Z. Analysis and optimization of the gear-shifting process for automated manual transmissions in electric vehicles. *Proc. Inst. Mech. Eng. Part D J. Automob. Eng.* **2017**, *231*, 095440701668546. [[CrossRef](#)]

22. Gao, B.; Lei, Y.; Ge, A.; Chen, H.; Sanada, K. Observer-based clutch disengagement control during gear shift process of automated manual transmission. *Veh. Syst. Dyn.* **2011**, *49*, 685–701. [[CrossRef](#)]
23. Li, G.; Grges, D. Optimal control of the gear shifting process for shift smoothness in dual-clutch transmissions. *Mech. Syst. Signal Process.* **2018**, *103*, 23–38. [[CrossRef](#)]
24. Jie, Y.; Zhu, G.G. Model predictive control of a power split hybrid powertrain. In Proceedings of the American Control Conference, Boston, MA, USA, 6–8 July 2016.
25. Xia, G.; Chen, J.; Tang, X.; Zhao, L.; Sun, B. Shift quality optimization control of power shift transmission based on particle swarm optimization–genetic algorithm. *Proc. Inst. Mech. Eng. Part D J. Automob. Eng.* **2022**, *236*, 872–892. [[CrossRef](#)]
26. Ghovvati, M.; Khayati, G.; Attar, H.; Vaziri, A. Comparison across growth kinetic models of alkaline protease production in batch and fed-batch fermentation using hybrid genetic algorithm and particle swarm optimization. *Biotechnol. Biotechnol. Equip.* **2015**, *29*, 1216–1225. [[CrossRef](#)]
27. Raquel, C.R.; Naval, P.C., Jr. An effective use of crowding distance in multiobjective particle swarm optimization. In Proceedings of the Genetic and Evolutionary Computation Conference, GECCO 2005, Washington, DC, USA, 25–29 June 2005.
28. Shi, X.H.; Wan, L.M.; Lee, H.P.; Yang, X.W.; Wang, L.M.; Liang, Y.C. An improved genetic algorithm with variable population-size and a PSO-GA based hybrid evolutionary algorithm. In Proceedings of the International Conference on Machine Learning & Cybernetics, Xi'an, China, 5 November 2003.
29. Hongchao, J. Shift Quality Control of Automatic Transmission for Off-Road Vehicle. Ph.D. Thesis, Beijing Institute of Technology, Beijing, China, 2018. [[CrossRef](#)]
30. Zhang, K.; Shen, C.; Liu, X.; Yen, G.G. Multi-Objective Evolution Strategy for Dynamic Multi-objective Optimization. *IEEE Trans. Evol. Comput.* **2020**, *24*, 974–988. [[CrossRef](#)]
31. Cheng, R.; Jin, Y.; Olhofer, M.; Sendhoff, B. Test Problems for Large-Scale Multiobjective and Many-Objective Optimization. *IEEE Trans. Cybern.* **2017**, *47*, 4108–4121. [[CrossRef](#)] [[PubMed](#)]
32. Xia, G.; Zong, H.; Tang, X.; Zhao, L.; Sun, B. Integrated control strategy of tractor hydromechanical continuously variable transmission. *Proc. Inst. Mech. Eng. Part D J. Automob. Eng.* **2021**, *235*, 649–671. [[CrossRef](#)]
33. Huang, L.Y.; Guan, K.S.; Xu, T.; Zhang, J.M.; Wang, Q.Q. Investigation of the mechanical properties of steel using instrumented indentation test with simulated annealing particle swarm optimization. *Theor. Appl. Fract. Mech.* **2019**, *102*, 116–121. [[CrossRef](#)]

Disclaimer/Publisher's Note: The statements, opinions and data contained in all publications are solely those of the individual author(s) and contributor(s) and not of MDPI and/or the editor(s). MDPI and/or the editor(s) disclaim responsibility for any injury to people or property resulting from any ideas, methods, instructions or products referred to in the content.